

4E3 Research Methods Assignment 2: Research Proposal

K. Bakhet¹, B. Gaffney¹, B. Lee¹, E. McAleese¹, F. O'Connor¹, M. Sadlier¹,

E-mails: **bakhetk@tcd.ie, brgaffne@tcd.ie, bilee@tcd.ie, mcaleeem@tcd.ie, foconno1@tcd.ie, msadlier@tcd.ie**

¹ Group Number 17,

November 2, 2025

Contents

| | | |
|----------|---|-----------|
| 1 | Introduction to Acoustic Liners for UAM Noise Reduction | 3 |
| 1.1 | Acoustic Liners for Aircraft Noise Reduction | 3 |
| 1.2 | Single-DOF vs Double-DOF Liners | 3 |
| 1.3 | State of the Art in DDOF Acoustic Liners | 4 |
| 2 | Physics | 4 |
| 2.1 | Overview and Design Objective | 4 |
| 2.2 | Noise Source Mechanisms | 4 |
| 2.3 | Initial Conditions and Test Rig Apparatus | 5 |
| 2.4 | Underlying Physical Mechanisms | 7 |
| 2.5 | How the Design Alters the Performance | 7 |
| 2.6 | Deriving an Impedance Model | 8 |
| 2.7 | Predicted Performance | 10 |
| 3 | Manufacturing Strategy | 13 |
| 3.1 | Physical Properties of Materials | 14 |
| 3.2 | MSLA Process Overview | 16 |
| 3.3 | Part Orientation and Supports | 16 |
| 4 | CAD Design of Finished Product | 18 |
| 4.1 | CAD Drawing: | 18 |
| 4.2 | Isometric View: | 19 |
| 4.3 | Summary of Our Design | 19 |
| 4.4 | Mass Properties | 19 |
| 5 | Risk Assessment | 20 |
| 5.1 | General issues with MSLA | 20 |
| 5.2 | Impact on Our Design and Schedule | 20 |
| 5.3 | Mitigation Plan | 21 |
| 6 | Appendix | 21 |
| 6.1 | MATLAB Script | 21 |
| 6.2 | Meeting 1 - Introductory Meeting | 26 |
| 6.3 | Meeting 2 - Design Clarification and Progress Updates | 27 |
| 6.4 | Meeting 3 - Final Review and Submission Planning | 27 |
| 7 | CRedit Author Statement | 28 |
| 8 | Generative AI Declaration | 29 |
| 9 | Group Grade Scaling Factor | 29 |

1 Introduction to Acoustic Liners for UAM Noise Reduction

Urban Air Mobility (UAM) vehicles, including electric vertical take-off, and landing (eVTOL) air taxis, are a rapidly emerging sector in the aviation industry that operate predominantly in close proximities to urban settings. NASA has noted that UAM operations will require extremely quiet performance near vertiports [1], which are typically in close proximity to noise-sensitive areas like large towns, and cities to avoid hindering their possible uses. Furthermore, the unique nature of UAM vehicles noise characteristics – strong tonal components, and rapid modulation – can make listeners perceived interpretation to be one of more annoyance than conventional sounds at similar sound levels [2]. These observations underscore the importance that effective noise mitigation strategies for UAM holds. Reducing rotor noise by even 10-15dB, is projected to dramatically lower the affected area, and the population exposed to high noise levels [3] highlighting a clear need for innovative noise reduction technologies in UAM designs.

1.1 Acoustic Liners for Aircraft Noise Reduction

Acoustic liners are well established passive noise control technology. They are widely used in aviation, particularly in aircraft engines to absorb sound in ducts. An acoustic liner typically consists of a resonant chamber, made up of a perforated facing sheet backed by an air cavity, which dissipates acoustic energy as heat through viscous losses [4]. In modern engines, acoustic liners are applied to the inner walls of engine intakes, and bypass ducts, and serve as the primary mechanism in noise. Generally, these liners operate on the principle of a Helmholtz resonator. The sound field in the duct couples into the cavity through the perforations, causing air trapped within to oscillate, and absorb sound at the resonant frequency. Traditionally, SDOF(single-degree-of-freedom) are efficient at attenuating noise, but only over narrow frequency bands. In the context of UAM rotors, which generate both broadband noise, and tonal blade-passing frequencies, a single cavity has limited effect [4]. Therefore, the challenge is to achieve broadband noise absorption, within the strict mass, and dimensional constraints of UAM vehicles. As UAM vehicle designs evolve, there is an increasing requirement for liners that provide broadband noise mitigation in a physically compact mechanism. Acoustic liners suitable for UAM vehicle application must therefore cover a wide frequency range, while maintaining a small size.

1.2 Single-DOF vs Double-DOF Liners

One method of broadening the absorption bandwidth is by using a multiple-DOF acoustic liner. An SDOF liner has only one cavity, or set of cavities, beneath the perforated faceplate. This yields a single resonant frequency. In contrast to this, a DDOF (double-degree-of-freedom), incorporates two resonant layers. It typically consists of a perforated faceplate, a first cavity, a second cavity, the septum which is a perforated sheet separating both cavities, and a rigid backplate [5]. This two-cavity configuration allows for two distinct resonant frequencies – one associated with the upper cavity, and the other with the lower – thereby extending the range of frequency over which sound can be absorbed. Simply put, the DDOF liner behaves as two Helmholtz resonators in series, each tuned to a separate frequency. The inclusion of the perforated septum between has been proven to greatly increase sound absorption performance, and broaden the bandwidth of attenuation [4]. In fact, modern aircraft engine nacelles rely on DDOF liner designs for broadband fan noise mitigation, as they are less sensitive to narrow tuning, and perform more robustly across different source conditions [5]. For UAM applications, where possible liner depth is heavily limited, these DDOF designs offer a solution to obtain broader noise reduction without compromising thickness. For example, Tang et al. demonstrated that two Helmholtz resonators – essentially a DDOF acoustic liner – produced two absorption peaks and a wider overall bandwidth of attenuation, when compared with a single cavity design with similar material, and geometry [6]. Therefore, leveraging a DDOF design for our proposed acoustic liner is a promising approach to meet the required noise reduction requirements within the compact size constraints.

1.3 State of the Art in DDOF Acoustic Liners

Extensive research, and development has occurred in recent years on multi-layer acoustic liners. In the aerospace industry, DDOF liners are predominantly utilised, and new fabrication techniques are expanding their capabilities. For instance, researchers have explored 3-D printed two-layer liners, with micro-perforated septa to enable abstract chamber geometries that can conform to curved ducts [5]. These advances aim to optimise acoustic noise reduction area, even in unconventional, and compact inlet geometries. Beyond engine nacelles, there are growing interests in the application of liners in rotorcraft, and UAM vehicle noise sources. NASA have begun evaluating acoustic liners inside ducts of tiltrotors, and lift fans [7]. This suggests the aerospace community now recognises acoustic liner technology as a viable noise reduction mechanism for UAM applications. Recent experimental work has also validated the benefits of liners. Palleja-Cabre et al. tested liner performance in a ducted fan setup, and achieved up to a 5dB reduction in overall sound pressure level, reducing both tonal blade, and broadband components [8]. These findings demonstrate that significant noise attenuation is achievable with a DDOF liner design, even at lower Mach numbers, and smaller scale geometries of UAM vehicles. The current state of the art in UAM noise reduction, therefore, comprises both design optimisation of a multi-DOF liner, for a broader bandwidth of absorption, and practical demonstrations of noise reduction in systems similar in nature to UAM vehicles. Given the above background, a DDOF acoustic liner is proposed as a solution to the annoyance of UAM rotor noise.

2 Physics

2.1 Overview and Design Objective

The physics behind how acoustic liners work and how noise is generated by UAM rotor blades will determine the final design of the acoustic liner. In the previous assignment, the physics of liner technologies and how noise is generated was discussed briefly. In this section, the physical phenomena will be explored in greater detail in an attempt to create a design that can efficiently attenuate sound waves, while also being lightweight, bio-inspired, cost effective, and easily manufactured. Various calculations will be performed to design a liner that can perform well in the test rig. The goal is to design an acoustic liner device using an additive manufacturing technique (3D printing) while adhering to various design conditions and constraints.

2.2 Noise Source Mechanisms

In the previous literature review, the physics of UAM noise generation was discussed. The noise is generated from a variety of different sound sources and the combined effect of each source produces a complex acoustic signature. Some of the sources include:

- **Tonal Noise:** A phenomenon that occurs due to periodic variations in the aerodynamic force loading from the blades' rotation. This generally occurs at low-speed flight.
- **Broadband Noise:** Produced by random layer turbulence such as boundary layer turbulence, flow separation, and wake instabilities. This generally occurs at higher flight speeds, and thus higher frequencies.
- **Blade-Vortex Interaction:** This arises when the a rotary blade intersects the tip vortex created by another blade, which generates pressure fluctuations and intense noise bursts.
- **Mechanical Noise:** Rotors and drive components can generate noise, and while this source is typically lower in amplitude, it does contribute to the overall complexity of the noise generated.

All of these noise sources combine to generate a complex sound signal. For the sake of accuracy and practicality, a test rig will be used to test the performance of our final liner design. Sound waves will be generated to replicate the varying frequencies and sound intensity of a UAM device's noise emission.

2.3 Initial Conditions and Test Rig Apparatus

To test the performance of the liner, a test rig known as an impedance tube will be used. It is an experimental apparatus used to test the sound absorption coefficient, transmission loss, and acoustic impedance of an acoustic liner. It works by generating a sound signal using a loudspeaker/driver. This sound wave travels down the tube towards the liner sample. Due to the narrow diameter of the tube, the sound behaves as a plane wave. When the wave hits the sample, part of it is reflected, and part of it is transmitted through the material. Four microphones are positioned within the apparatus, two on each side of the sample, and measure the acoustic pressure at four known positions. From these microphones, the incident and reflected wave components and the reflection and transmission coefficients can be calculated. From these data points, the absorption coefficient and acoustic impedance of the liner can be determined.

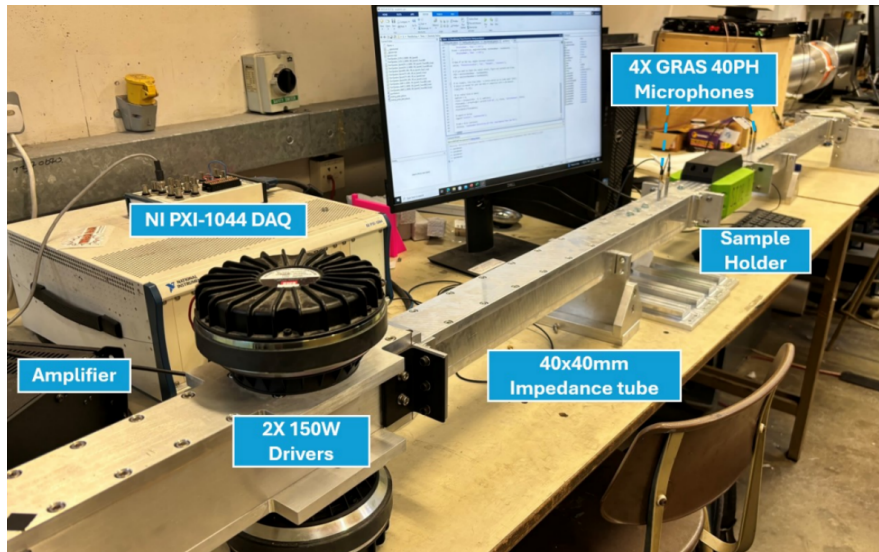


Figure 1: Photograph of the apparatus setup being used to test the performance of our final liner design [9].

In this particular setup, the sound is generated by two 150 W drivers. These are powerful loudspeakers mounted at one end of the tube. Their function is to generate controlled sound waves that travel through the tube. The NI PXI-1044 DAQ is a device used to generate output signals to the amplifier and also records microphone outputs. The amplifier is used to boost the signal from the DAQ and drive the speakers. Once the sound waves are generated, the 40 x 40 mm impedance tube guides the waves and propagates them as plane waves. The liner sample (the green block in the above image) is held in the sample holder. There are two GRAS 40 PH microphones placed at each side of the liner sample to allow for accurate data collection. This data is then fed to the computer, where a MATLAB script is used to analyse the acquired data and calculate reflection, transmission, and absorption.

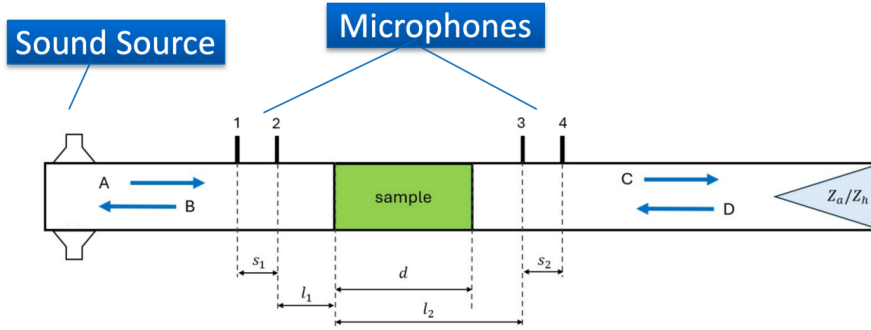


Figure 2: Schematic of the basis of the test apparatus [9].

6

Upon contacting Dr. John Kennedy, the group was advised to use a frequency range of 300 - 3000 Hz. This is a sufficient range for testing the performance of a liner for UAM applications. However, it is worth noting that due to the apparatus setup, the upper frequency limit is governed by the impedance tube walls through the cut-off frequency. In this application, the cut-off frequency is the maximum frequency at which sound in an impedance tube behaves as a simple plane wave. Once it is greater than this frequency, the sound becomes multi-dimensional and complex, meaning that it cannot be analysed using plane-wave acoustic theory.

Assuming that the speed of sound in air at 20° is approximately 343 m/s and the impedance tube dimensions are 40 x 40 mm (a x b):

$$f_c = \frac{c}{2} \sqrt{\left(\frac{1}{a}\right)^2 + \left(\frac{1}{b}\right)^2} = \frac{c}{2a} = \frac{343}{2(0.04)} = 4287.5 \text{ Hz} \quad (1)$$

Therefore, this cut-off frequency justifies 300 - 3000 Hz as being a practical testing range.

As a group, we decided that we would aim to achieve acoustic absorption for a range in or around 500 - 1000 Hz.

When designing the liner, there are also multiple other physical constraints that need to be considered. In order for the liner sample to fit in the test rig, it must be 37 mm deep, 40 mm wide, and up to 160 mm long.

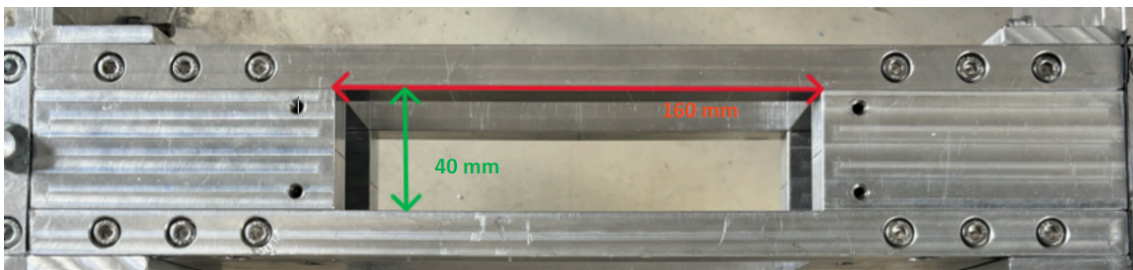


Figure 3: Photograph of the holding block for the liner sample in the apparatus [9].

From our previous assumption that the speed of sound in air within the impedance tube is 343 m/s, the range of wavelengths that need to be attenuated can be calculated.

$$c = f\lambda \quad (2)$$

The sound wavelength ranges from 0.1143 to 1.143 m for a frequency range of 300 to 3000 Hz, respectively.

There is also a limitation from an additive manufacturing point of view. The 3D printer that we are using to manufacture our liner is a Prusa Mini+. This is a fused deposition modelling (FDM) printer used to print polymers, and can achieve a layer height of 0.01 mm.

2.4 Underlying Physical Mechanisms

The operation of an acoustic liner is governed by the combination of several fundamental acoustic phenomena. The goal is to create a system that can enable the conversion of incident acoustic energy into heat, thereby reducing the amplitude of the reflected pressure waves and achieve broadband attenuation.

In order to design a liner that can attenuate waves successfully, a key parameter is the impedance. Acoustic impedance is a property of a medium that describes how much resistance it offers to a sound wave. It is calculated by multiplying the medium's density by the speed of the sound wave passing through it. The goal is to create a liner that can perform a phenomenon known as impedance matching. This occurs when the impedance of the liner is as close to that of the sound waves being directed at it. The goal is to minimise reflections from the liner.

$$Z_{\text{liner}} \approx \rho_0 c_0 \quad (3)$$

The basis for how an acoustic liner works is through the Helmholtz Resonance phenomenon. A Helmholtz Resonator is built on this phenomenon. It is defined as a system consisting of a chamber with rigid walls connected to a constricted duct, which exhibits a dynamic regime where mass and stiffness effects are uncoupled, acting as a spring-mass system. It resonates at a frequency significantly lower than the diffraction frequency of the surrounding medium [10]. Helmholtz resonance occurs when the air in the moving neck of the liner acts like a moving mass, and the air in the cavity acts like a mechanical spring (compressing and expanding), ultimately creating a spring-mass system that can oscillate at a specific natural frequency. The peak attenuation occurs when resonance is achieved. By changing the neck diameter, the porosity, or cavity depth certain resonances can be tuned.

The formula for the Helmholtz frequency of a Helmholtz resonator can be given by:

$$f_H = \frac{c_0}{2\pi} \sqrt{\frac{A}{VL_{\text{eff}}}} = \frac{c_0}{2\pi} \sqrt{\frac{\phi}{LL_{\text{eff}}}} \quad (4)$$

where c_0 is the speed of sound, A is the neck cross-sectional area, V is the cavity volume, L_{eff} is the effective neck length, ϕ is the porosity, and L is the cavity depth.

Viscous and thermal damping is also a key phenomenon that governs how an acoustic liner works. When an acoustic wave interacts with a solid boundary or passes through a perforated liner, velocity and temperature gradients form within a thin boundary layer adjacent to the wall. Within this layer, viscous shear stresses and thermal conduction act to dissipate acoustic energy, converting oscillatory kinetic and pressure energy into heat.

2.5 How the Design Alters the Performance

To ensure that the acoustic liner can successfully attenuate sound waves, the physics behind how it works needs to be verified. The main operating principle of an acoustic liner is the conversion of acoustic energy into heat through viscous friction and thermal conduction in the small passages (perforations, pores, or necks) and in the air within the cavity. When sound waves force air to oscillate through the small holes and cavities within the liner, the mechanical energy of the wave is converted to thermal and viscous energy that is dissipated through the walls, ultimately reducing the amplitude of the reflected sound wave and producing sound absorption [11].

The liner we have chosen to design is a double-degree-of-freedom (DDOF) liner. It uses a micro-perforated panel (MPP) on the upper surface, combined with square-shaped cavities and cylindrical necking, taking inspiration from biomaterials that have successfully been proven to attenuate sound wave frequencies. By using a DDOF, we will utilise two cavities of different depths each tuned to difference resonances. This broadens the absorption band, which ideally should cover the target range with overlapping resonances.



Figure 4: SDOF liner with an MPP faceplate [12].

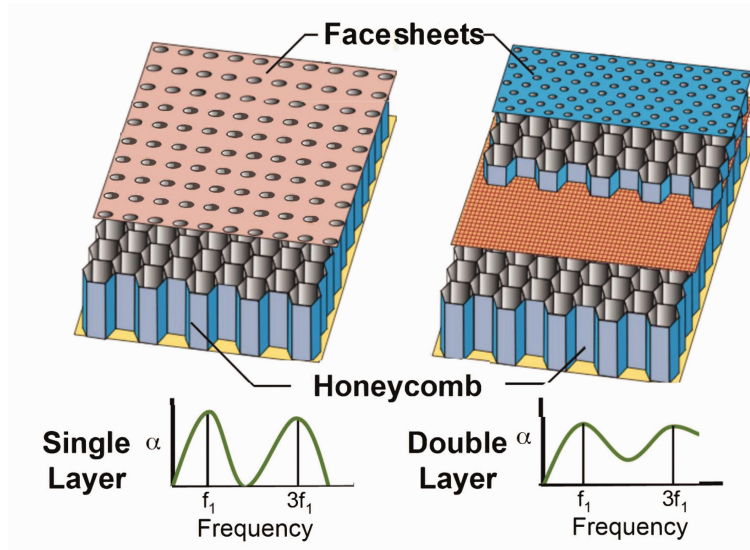


Figure 5: Difference in absorption coefficients with respect to frequency for SDOF vs DDOF [13].

For a DDOF liner, a DDOF impedance chain is required (facesheet MPP + cavity 1 + perforated septum + cavity 2). To simplify the idea of a DDOF liner, we can think of it as an electrical circuit. The liner can act in either a series or parallel fashion. By having a DDOF liner, it makes it easier to target a more broadband frequency spectrum. As a group, we considered using a MDOF liner, that used different cavity depths and hole diameters, but for the sake of the assignment we felt it would be better to just choose a frequency band and achieve high absorption.

2.6 Deriving an Impedance Model

As stated, the goal was to design an acoustic liner device that is capable of attenuating a broadband of frequencies from 500 to 1000 Hz. To do this, a methodical process involving a lot of research was carried out. The initial conditions listed above gave some initial and boundary conditions. Much of the formulae, derivations, and research used in this section was conducted by other authors, who will be accredited.

To start, a general model was built using some initial conditions.

- Maximum liner depth = 37 mm.
- Minimum layer size = 0.01 mm.

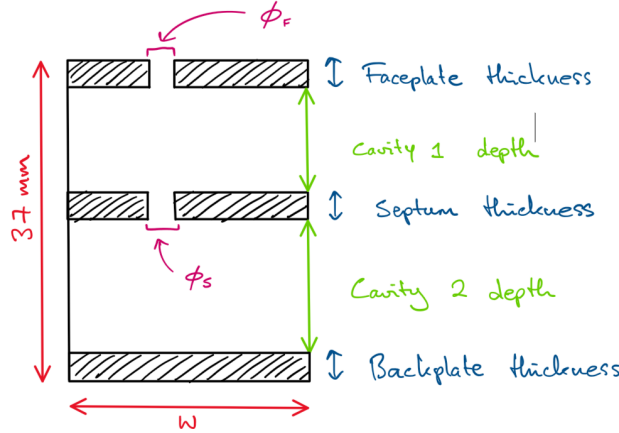


Figure 6: Sketch of proposed liner design.

To build an impedance model of the liner system, an impedance chain is needed. An impedance chain is a series of acoustic layers whose combined impedance determines how an incidence sound wave interacts with the surface. Each layer has its own acoustic impedance, Z_i , that depends on its geometry and material. Impedance chains are a key performance characteristic of DDOF liners, and is what enables them to achieve broadband attenuation. To create this model, each layer can be treated as its own impedance.

The formula used to calculate the impedance of an MPP faceplate was derived from Maa's 'Theory and Design of Microperforated Panel Sound-Absorbing Constructions, 1974' [14]. Maa's work on MPP absorber theory transformed sound absorber design by introducing a purely structural, fibre-free, and analytically predictable model for broadband acoustic attenuation. The formula that he derived to model the acoustic impedance of an MPP faceplate can be given as:

$$Z_{\text{MPP}} = -Z_0 \left(\frac{i \omega \rho_0 J_0 \left(\frac{D}{2} \sqrt{\frac{-i \omega}{\nu_0}} \right)}{c_0 \phi J_2 \left(\frac{D}{2} \sqrt{\frac{-i \omega}{\nu_0}} \right)} \right) [T + 0.85 D \cdot \Psi(\phi)] \quad (5)$$

where ϕ is the porosity of the microperforated plate, J_0 and J_2 are the zeroth- and second-order Bessel functions, and ν_0 is the kinematic viscosity of air. The values T and D are the plate thickness and perforation diameter, respectively [15]. Finally, $\Psi(\phi)$ is the Fok function, which is used to determine the hole-to-hole interactions and is given by

$$\Psi(\phi) = \sum_{F=0}^a a_F \left(\sqrt{\phi} \right)^F \quad (6)$$

The above equations, J_0 and J_2 , are known as the zeroth and second order Bessel functions [15]. They are functions that are used to solve problems with cylindrical or spherical symmetry, in applications such as heat transfer, acoustics, and vibrations. Due to their complex nature, they can be solved easily using computation software such as MATLAB.

$$J_0 \left(\frac{D}{2} \sqrt{\frac{-i \omega}{\nu_0}} \right); J_2 \left(\frac{D}{2} \sqrt{\frac{-i \omega}{\nu_0}} \right) \quad (7)$$

The impedance of the first cavity can be treated using an impedance formula for closed termination:

$$Z_e = -i\rho_0 c_0 \cot(k_0 L_c) \quad (8)$$

where L_c is the cavity depth and k_0 is the wave number derived from angular frequency:

$$k_0 = \frac{2\pi f}{c_0} = \frac{\omega}{c_0} \quad (9)$$

The impedances of the septum and the second cavity can be found similarly to above, but by using the values for septum porosity, thickness, diameter, and the depth of the second cavity.

This DDOF liner system creates the following series/parallel impedance chain:

$$Z_{total} = Z_{MPP} + Z_{in} \quad (10)$$

Where Z_{in} , [11], is the input impedance looking into cavity 1, represented as:

$$Z_{in,1} = Z_0 \frac{Z_{load} \cos(kL_1) - j Z_0 \sin(kL_1)}{Z_0 \cos(kL_1) - j Z_{load} \sin(kL_1)} \quad (11)$$

$$Z_{load} = Z_{septum} + Z_{cavity2} \quad (12)$$

Taking this value for total impedance, the absorption coefficient of the liner can be found.

$$\alpha = 1 - \left| \frac{Z_{total} - Z_0}{Z_{total} + Z_0} \right|^2 \quad (13)$$

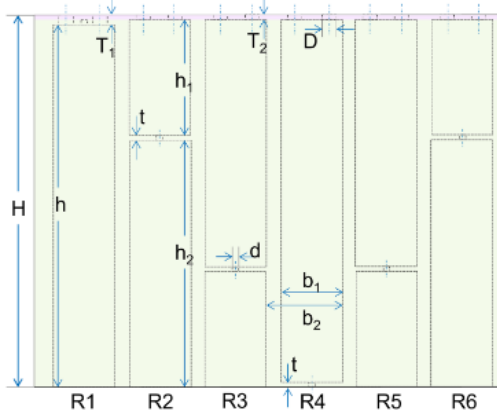
The average absorption for the liner can be found by integrating the absorption over a specified frequency range.

$$\bar{\alpha} = \frac{1}{\omega_2 - \omega_1} \int_{\omega_1}^{\omega_2} \alpha(\omega) d\omega \quad (14)$$

To design our liner, the above equations were taken and implemented into a MATLAB model to simulate acoustic behaviour. The equations used were derived/adapted from a variety of research papers and fundamental theories used to describe acoustic behaviour: [16], [15], [14], [11].

2.7 Predicted Performance

To design the liner, we took reference and inspiration from other papers that took a similar approach. By building a model in MATLAB, we were able to take the initial conditions given in these papers and refine them by changing variables to try and create a model that works. We took our initial conditions from the paper, "Evaluating an Additive Manufactured Acoustic Metamaterial Using the Advanced Noise Control Fan" [16].



(a)

| Parameter | Value, mm |
|-------------------------------------|-----------|
| Total core height, h | 50 |
| Upper duct height, $h_{1,R2}$ | 12.35 |
| Lower duct height, $h_{2,R2}$ | 37.25 |
| Duct internal width, b_1 | 5.6 |
| Duct total width, b_2 | 6 |
| Faceplate thickness, T_2 | 0.5 |
| Septum thickness, t | 0.2 |
| Faceplate perforation diameter, D | 0.63 |
| Faceplate perforation count, N | 416 |
| Septum perforation diameter, d | 0.4 |

(b)

Figure 7: Example diagram and reference values used to build the impedance model [16].

From this data, we took the below initial conditions for testing our liner. The cavity depths had to be adjusted proportionally to accommodate for the depth restriction of 37 mm.

Despite not being able to obtain an exact figure for the porosity from references, we determined faceplate and septum porosity, ϕ_2 and ϕ_1 , to be 0.02. Using these values and plugging them into a MATLAB model based on the equations given, we determined the following:

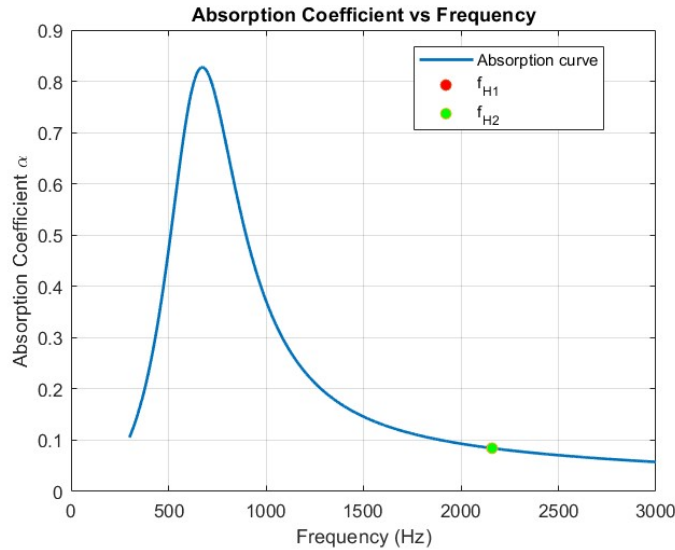


Figure 8: Graph of the absorption coefficient vs frequency for our given initial conditions.

```

Total liner depth is 0.037 mm
Frequency band 1 = 2158.8413 Hz
Frequency band 2 = 2160.3136 Hz
The average absorption coefficient of the liner is: 0.22675

```

Figure 9: Terminal output for simulation using our initial conditions.

The MATLAB results indicate strong acoustic absorption between approximately 500 Hz and 1000 Hz, followed by a decline at higher frequencies. The model predicts two Helmholtz resonance frequencies at

2.159 kHz and 2.160 kHz, which are effectively coincident. This suggests that the system behaves as a single effective resonator, rather than exhibiting two distinct resonance modes.

This overlap likely arises because the liner depth is insufficient to support two acoustically distinct cavities; in other words, the total depth is too small relative to the wavelengths involved to produce separate resonance peaks.

To investigate this, several geometric and material parameters were varied in the model in an attempt to achieve a broader absorption bandwidth. While it was possible to spread the absorption over a wider frequency range, the peak absorption amplitude decreased significantly, indicating a trade-off between bandwidth and absorption magnitude.

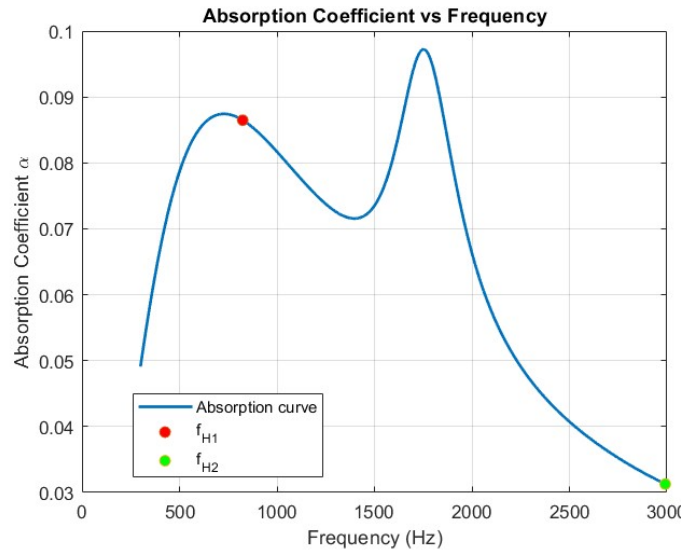


Figure 10: Graph of the absorption coefficient vs frequency for a larger bandwidth model.

```
Total liner depth is 0.037 mm
Frequency band 1 = 701.8375 Hz
Frequency band 2 = 2991.5215 Hz
The average absorption coefficient of the liner is: 0.054747
```

Figure 11: Terminal output for simulation using a larger bandwidth model.

Based on this conclusion, we were able to derive our dimensions for the liner:

| Parameter | Value, mm |
|-----------------------------------|-----------|
| Liner depth, H | 37 |
| Faceplate thickness, T_2 | 0.5 |
| Faceplate perforation diameter, D | 0.63 |
| Cavity 1 depth, h_1 | 12.35 |
| Septum thickness, t | 0.2 |
| Septum perforation diameter | 0.4 |
| Cavity 2 depth, h_2 | 23.65 |
| Backplate thickness, T_2 | 0.5 |

Table 1: Final dimensions of our proposed liner design based on calculations.

The number of holes and cavities influences the performance of the liner massively. Since each hole/cavity combination acts as a Helmholtz resonator, the more features there are, mean an increased surface interaction.

This means that there is a larger overall boundary area where losses can occur, and thus greater total energy absorption. The more holes there are, the closer the liner's impedance is to that of air. This reduces the reflection of the incoming sound wave, and increases the absorption.

Another design feature we were looking at was using multiple holes and cavities of different depths and widths. This would enable the liner to hypothetically attenuate a much broader frequency band, however seeing as we put significant focus on attenuating waves in the 500-1000 Hz, this was not done. Ideally we would be able to do this iteratively by varying each dimension and running simulations, but this would be highly computationally and time intensive for the sake of this assignment.

While increasing the overall porosity and air content of the liner may be good for performance, it does come with its downsides. Too many holes and cavities can compromise the structural integrity of the liner, allow air to flow too freely which will ultimately reduce the resonance effect, and decrease the overall absorption if the air does not trap the air effectively.

Based on these considerations, our dimension constraints (160 x 40 x 37 mm), and some research, we decided to use a total of 156 holes in a 26 x 6 configuration.

The design shown in the below sketch, consists of a perforated faceplate (with 0.63mm perforations), beneath this is two internal cavities – an upper cavity of 12.35mm in height, and a lower one of 23.65mm – separated by an internal septum with 0.4mm diameter perforations, and finally a rigid backplate. The length, width, and height are determined by the dimensions of the testing apparatus which will be used. This configuration is informed directly by the state-of-the-art literature reviewed above, and subsequent mathematical analysis performed in this paper. The two resonant cavities give allow for sound absorption over wider frequency ranges, targeting tonal, and broadband noise components. The relatively small overall geometry aligns with spatial concerns for application in UAM ducted fan installations, while the presence of perforated sheets provides the necessary acoustic resonance without the need for bulky materials. The viability of this design is affirmed by our findings from Assignment 1, which identified broadband passive liners as a key tool for noise mitigation in UAM, and showed that a dual resonator liner could meet necessary noise reduction targets within size constraints [3]. By drawing on the established best-in-class practices from engine nacelle liners, and tailoring the geometry to UAM-specific constraints, this design is well justified as a high potential solution in reducing overall UAM noise.

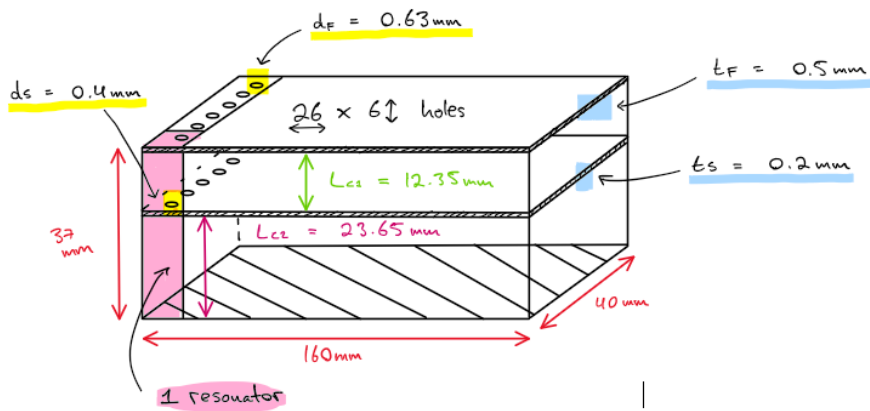


Figure 12: Design Sketch of Proposed Acoustic Liner

3 Manufacturing Strategy

For the manufacturing of the UAM acoustic liner, there are three main 3D printing technologies available for use in the Parsons Lab. These are:

- Extrusion-based Fused Deposition Modelling (FDM)
- Resin-based Masked Stereolithography (MSLA)
- Powder-based Selective Laser Melting (SLM)

3.1 Physical Properties of Materials

The choice of materials for the UAM acoustic liner is critical for achieving the desired acoustic performance, structural integrity, and manufacturability. The physical properties of the liner material primarily density, stiffness, acoustic impedance, and thermal stability. This determines how effectively it can absorb sound, resist deformation under load, and maintain the precision of its micro features. The liner walls should act acoustically rigid with respect to air so that the sound energy is not dissipated by vibration of the liner's solid structure but rather by viscous and thermal loss within the air cavities [17].

3.1.1 Base Material – Photopolymer Resin (MSLA)

A UV-curable photopolymer resin has been selected as the base material for this project. The Masked Stereolithography (MSLA) process has been chosen for manufacturing with this material because the surface finish, geometric accuracy and feature resolution is superior to processes based on extrusion[18]. MSLA employs liquid resin which when subjected to UV light, it polymerises. MSLA has fine detail suitable for the micro-perforated faceplate (0.63 mm holes) and the perforated septum (0.40 mm holes)

Typical mechanical and thermal properties of the cured photopolymer resin are summarised below [18].

| <i>Property</i> | <i>Typical Value</i> | <i>Units</i> |
|-------------------------------------|----------------------|-------------------|
| <i>Density</i> | 1.1 – 1.2 | g/cm ³ |
| <i>Young's Modulus</i> | 2 – 3 | GPa |
| <i>Tensile Strength</i> | 50 – 70 | MPa |
| <i>Glass-Transition Temperature</i> | 70 – 80 | °C |
| <i>Shore D Hardness</i> | 80 – 85 | — |

Table 2: Typical mechanical and thermal properties of the cured photopolymer resin [18].

The properties guarantee that the liner remains stiff, dimensionally stable during acoustic testing, with a low overall mass. This is an important factor for UAM systems where every gram matters in energy consumption and payload efficiency. The structure will be treated as an acoustically rigid boundary (due to its relatively high modulus) for Helmholtz resonance. The smooth surfacing and medium densities also help in reducing the unintentional scattering or dampening effects among lining cavity [18] [17].

The chosen solution for this prototype was the acrylic-based MSLA photopolymer resin but several alternatives were shortlisted based on their sonic behaviour, manufacturability and mechanical property levels. Common 3D-printable thermoplastics include metal alloys and advanced resins.

3.1.2 FDM Polymers

Thermoplastics like PLA, poly-lactic acid and ABS, acrylonitrile butadiene styrene are commonly used thermoplastics in fused deposition modelling (FDM) printers due to their low prices and easy availability. These materials typically have densities of 1.2–1.3 g/cm³ and Young's moduli around 2–3 GPa, similar to photopolymer resins [19].

FDM produced parts tend to have poor surface finish, presence of interlayer porosity, and dimensional inaccuracy particularly with features smaller than 0.5 mm. Due to these limitations, cavity geometry is poorly

controlled, and acoustic leakage can occur between chambers, undermining liner impedance characteristics. The minimum feature size achievable with standard FDM nozzles (≈ 0.4 mm) which makes it impractical for producing the fine perforations required for broadband absorption [19].

As a result, FDM polymers while usable for initial scale prototypes are not suitable for DDOF acoustic liner which requires precision.

3.1.3 SLM Metal Alloys

Manufacturing using Selective Laser Melting (SLM) made of metallic powders AlSi10Mg and Ti6Al4V results in components that are very stiff and thermally stable [20].

Typical material properties are as follows :

AlSi10Mg: Density = 2.70 g/cm³, E = 70 GPa, Tensile Strength = 400 MPa

Ti6Al4V: Density = 4.43 g/cm³, E = 110 GPa, Tensile Strength = 900 MPa

propulsion environments typically create aerodynamic and thermal loads. Metals provide recommended stiffness-to-weight ratios and thermal resistance for maintaining dimensional stability under such loads. Nonetheless, these materials are costly, require post-processing, and have longer build times. To achieve accurate sub-millimetre holes using SLM requires high energy laser systems and tight process control [20].

Nonetheless, metallic liners represent a promising future direction for UAM noise reduction applications where temperature and structural loading exceed the limits of polymer-based materials.

3.1.4 SLA and Engineering Resins

Resins for Advanced Stereolithography (SLA) provides in mechanical and thermal performance. Flexible photopolymers (E \approx 0.5–1 GPa) can introduce enhanced damping, potentially reducing structural resonance; however, excessive flexibility can lower acoustic efficiency by absorbing sound energy within the walls themselves [21].

Conversely, high-temperature resins, often ceramic-filled or composite-based, can withstand temperatures up to 150–200 °C while maintaining mechanical rigidity. Materials of this sort would be useful for properly operating full-scale acoustic liners, especially those near engine ducts or lift-fan housings which heating and pressure variations are larger.

3.1.5 Summary of Material Comparison

| Property | MSLA Resin | PLA (FDM) | AlSi10Mg (SLM) | High-Temp SLA Resin |
|------------------------------------|-----------------------------|-----------------------|-----------------------------|---------------------|
| Density (g/cm ³) | 1.15 | 1.24 | 2.70 | 1.35 |
| Young's Modulus (GPa) | 2.5 | 3.0 | 70 | 3–4 |
| Tensile Strength (MPa) | 60 | 65 | 400 | 90 |
| Glass Transition Temp (°C) | 75 | 60 | 250 | 150 |
| Print Resolution | Excellent (≤ 0.05 mm) | Moderate (0.2–0.4 mm) | Excellent (≤ 0.05 mm) | Excellent |
| Surface Finish | Smooth | Rough | Smooth | Smooth |
| Suitability for Micro-Perforations | High | Low | High | High |
| Cost & Availability | Low | Very Low | High | Medium |

Table 3: Comparison of mechanical and physical properties for potential liner materials considered in this project.

[18, 19, 20]

According to the above comparison, the UV-curable photopolymer resin which is printed using MSLA offers the best combination of accuracy, stiffness and manufacturability for the acoustic liner. Its superior surface resolution allows for precise perforation geometry, and its moderate modulus helps maintain structure under acoustic loading. While metallic alloys and high-temperature resins are more durable and heat-resistant, they are outside the project's budget and timescale.

Future iterations could consider these alternative materials for the operation of UAM environments, such as in high-power or high-temperature ducts.

3.2 MSLA Process Overview

As this acoustic liner is to be investigated experimentally, resin-based Masked Stereolithography (MSLA) has been selected as the most suitable manufacturing process due to its high resolution and quality when compared to the alternative 3D printing technologies available for this project. MSLA is also typically faster than the alternatives, which is a major consideration for the manufacturing of our acoustic liner due to the tight time constraints of this project.

MSLA is a resin-based 3D printing technology that uses liquid resins that harden when exposed to certain wavelengths of light, typically ultraviolet. The printing material used is a liquid photopolymer resin stored in a shallow vat. Beneath the transparent resin vat there is an array of LED light sources, above which is an LCD screen that acts as a digital mask. The LCD screen displays a black and white image corresponding to one layer of the 3D model. The UV light passes through the white or transparent parts of the LCD screen and hardens the resin in the shape of the current layer. After each layer, the platform is lifted slightly, allowing more resin to flow underneath the hardened resin before curing the next layer, and so on. When cured, the photopolymer has suitable properties for the purpose of this investigation [22].

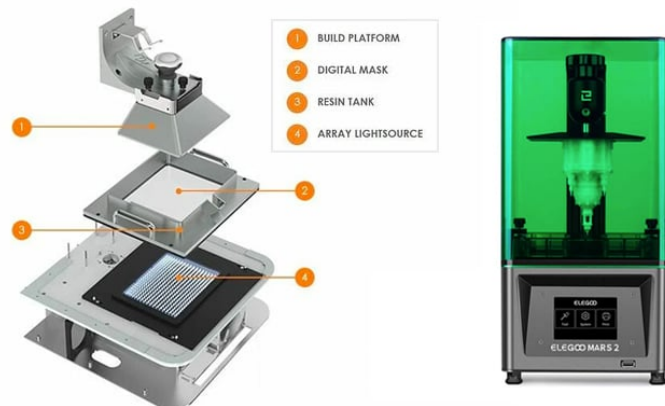


Figure 13: An illustration of how MSLA 3D printing works [23].

3.3 Part Orientation and Supports

As there are unsupported elements in the acoustic liner design, some supports will be necessary. To reduce the number of supports required during the manufacturing of the part, it is proposed that the acoustic liner be oriented at a 45° angle. This orientation helps to ensure there are no unsupported horizontal elements, which can often lead to build failures [22].

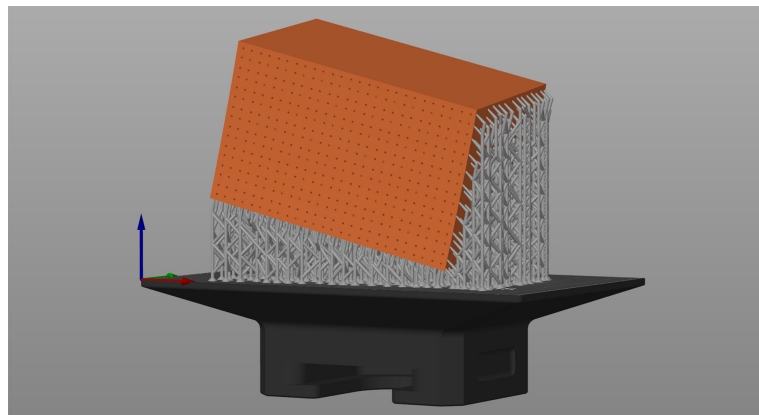


Figure 14: Example of the print process for the liner [16].

4 CAD Design of Finished Product

4.1 CAD Drawing:

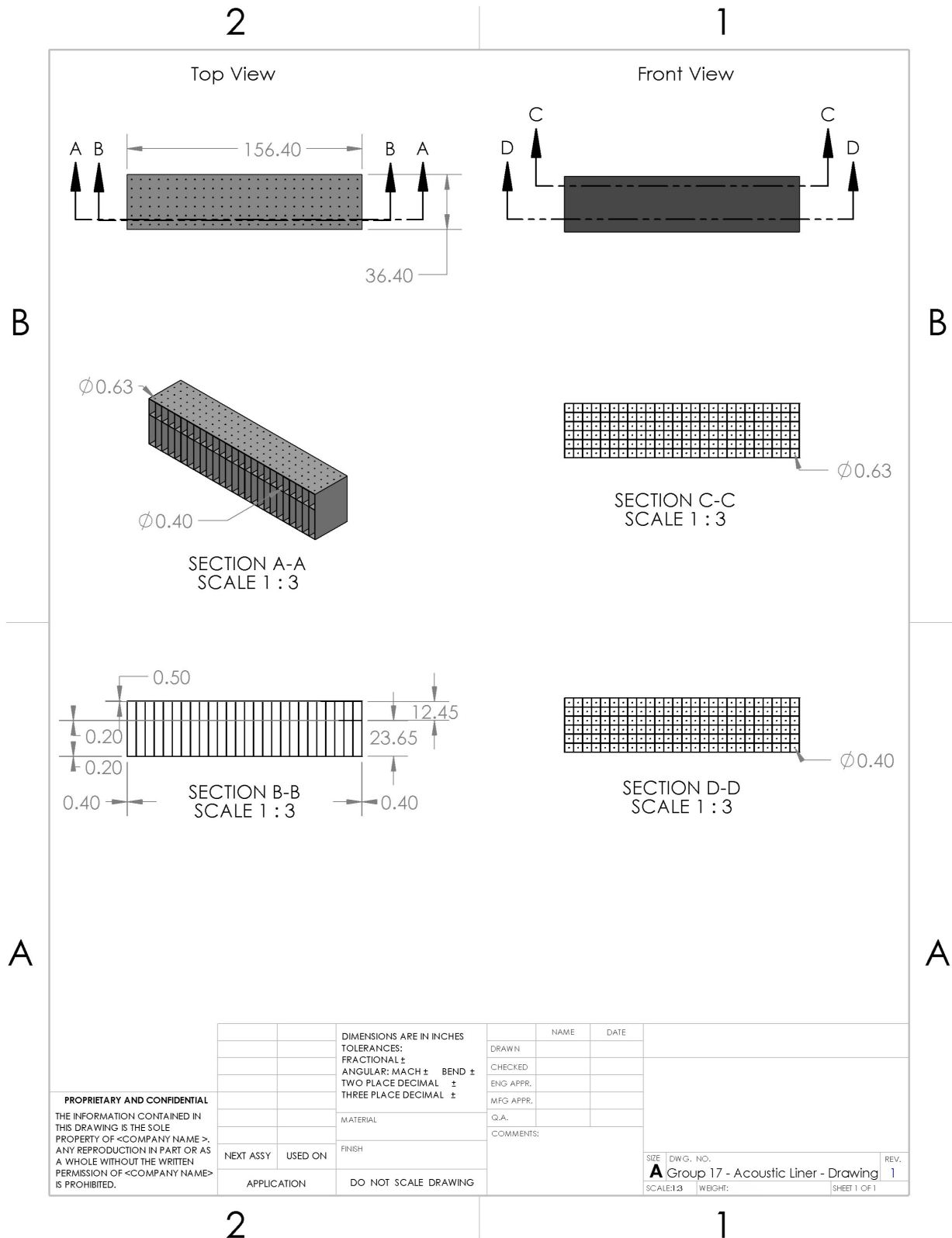


Figure 15: Solidworks drawing of our CAD design with included dimensions

4.2 Isometric View:

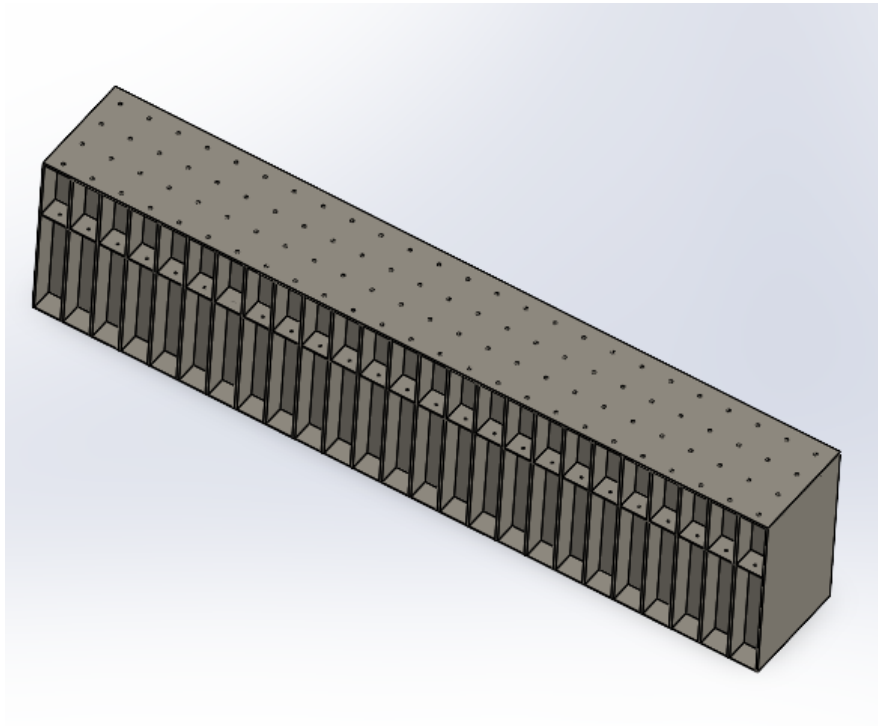


Figure 16: Isometric View of our CAD design

4.3 Summary of Our Design

Our liner is designed as a double degree of freedom (DDOF) acoustic attenuator, consisting of two perforated face sheets and two chambers of different depths. The upper face sheet comprises a 26×6 hole array, with each cylindrical hole machined to a diameter of 0.63 mm. The lower face sheet uses the same hole pattern (26×6), but with a reduced hole diameter of 0.40 mm. The upper chambers are 12.45 mm deep, and the lower chambers are 23.65 mm deep.

Each chamber is separated by internal walls with a thickness of 0.40 mm. The liner base thickness is 0.20 mm, and the perforated septum is also modelled with a thickness of 0.20 mm. For both the upper perforated plate and the perforated septum, the cylindrical holes are drilled through the centre of each square chamber.

To ensure proper fit within the test housing, dimensional tolerances were applied to the liner during the CAD design. The final adjusted dimensions for manufacture are 156.4 mm \times 36.4 mm \times 37 mm, as shown in Figure 15.

4.4 Mass Properties

Using the MSLA resin material properties defined above, a custom material was created in SolidWorks to obtain the mass properties of the liner.

```

Mass properties of Group 17 - Acoustic Liner
Configuration: Default
Coordinate system: -- default --

Density = 0.001150 grams per cubic millimeter

Mass = 39.104955 grams

Volume = 34004.308779 cubic millimeters

Surface area = 171426.719809 square millimeters

Center of mass: ( millimeters )
  X = 0.000000
  Y = -17.573495
  Z = 0.000000

```

Figure 17: Mass Properties of our liner using the custom material properties referenced above

5 Risk Assessment

Our manufacturing approach cannot be regarded as perfect because there is limited data to isolate the ways in which additive manufacturing alters liner acoustics. Given the limited time, we determine the main risks brought by MSLA. Because the advantages and disadvantages of MSLA are still under investigation and there is only limited knowledge available on the optimal design of components using this young process [22], a clear mitigation strategy is outlined and applied directly to the design measurements established earlier in the report.

5.1 General issues with MSLA

Internal features frequently print undersize because of light spread and over-cure with grooves < 0.4 mm and bores < 0.7 mm tending to close, causing IPA and post-curing cleaning to be required [22]. Pressure-equalising drain holes (≈ 4 mm for one and ≈ 3 mm for two, positioned at the lowest point) are advised because enclosed volumes can trap resin and result in “suction-cup” peel failures [22]. Photopolymerisation and UV post-cure shrinkage can generate residual stresses that can distort thin plates. Material and exposure choices alongside controlled post-cure can help limit this [24]. A combination of shrinkage and geometric deformation was found to cause MSLA to perform poorly in previous characterisation work, highlighting the necessity of controlling post-cure and confirming as-built geometry [25]. The general AM findings on surface roughness and dimensional tolerances apply to MSLA because it is a vat-photopolymerisation form of additive manufacturing. Roughness by itself does not fully explain model–experiment mismatch, and these effects can shift resonances and increase viscous losses, which raise flow resistivity/tortuosity [26], [27], [28], [25].

5.2 Impact on Our Design and Schedule

These variables shape both the performance of the liner and the way we build the liner. Due to limited build slots, schedule pressure is primarily focused on post-processing and first-time print success. The risk of reprints may arise when perforations emerge closed or undersized and additional cleaning or recure time is needed [22]. Our dimensions are within the guidelines, but there is a small margin of error. The 0.4 mm septum holes coincide with the documented threshold that requires careful over-sizing and clearing to open the printed, and the 0.63 mm faceplate holes are below the 0.7 mm safe zone, necessitating compensation and quality assurance [22]. Since the current design lacks drains, the enclosed volumes can retain resin during peeling or washing, increasing the clean-up time and the possibility of peel artifacts [22].

5.3 Mitigation Plan

Since internal features in MSLA tend to print undersize, due to over-cure and incorrect groove and bore geometry, slightly increasing the current design geometry can help build a larger manufacturing margin. This would help mitigate the risk of hole closure, helping to reduce rework and delays [22]. To improve cleaning and reduce the effects of the peeling suction cup, drains could be added to a non-acoustic face. Ideally, these drains would be positioned at the lowest point in the selected orientation. This would be approximately ≈ 4 mm if using a single drain or ≈ 3 mm if using two drains [22]. Features can be sealed during finishing (e.g., with sealants/primers) following washing and UV post-cure to ensure that additional drains do not affect the acoustic path [24]. To limit shrinkage-induced warping in thin plates, careful IPA cleaning and adequate UV post-cure could help minimise polymerisation-shrinkage stressed during curing [22], [24]. To reduce roughness that might have negative acoustic impacts on the design, use the same post-processing workflow: remove uncured resin with a thorough IPA clean and harden the surface with a full UV post-cure. If permitted on non-acoustic faces, apply light surface finishing or coatings (such as primers or sealants) to smooth asperities and enhance the final surface quality [24], [25].

6 Appendix

6.1 MATLAB Script

```
1 close all; clear; clc;
2
3 %% ----- Initial Conditions -----
4 % Constants
5 c0 = 343; % Speed of sound in air at 20 °C [m/s]
6 rho0 = 1.225; % Air density [kg/m^3]
7 Z0 = rho0 * c0; % Characteristic impedance of air [Pa·s/m]
8 v0 = 1.506e-5; % Kinematic viscosity of air [m^2/s]
9
10 % Frequency range
11 f = 300:1:3000; % [Hz]
12 omega = 2*pi*f;
13 k = omega / c0;
14
15 % Geometry constraints
16 max_liner_depth = 0.037; % [m] (37 mm maximum)
17
18 % Faceplate (micro-perforated panel)
19 faceplate_thk = 0.0005; % [m]
20 faceplate_d = 0.00063; % Hole diameter [m]
21 faceplate_phi = 0.02; % Open area ratio [-]
22 L_eff_faceplate = faceplate_thk + 0.85*faceplate_d;
23
24 % Cavity 1
25 cavity1_depth = 0.01235; % [m]
26
27 % Septum (perforated)
28 septum_thk = 0.0002; % [m]
29 septum_d = 0.0004; % Hole diameter [m]
30 septum_phi = 0.02; % Open area ratio [-]
31 L_eff_septum = septum_thk + 0.85*septum_d;
32
33 % Cavity 2
```

```

34 cavity2_depth = 0.02365;           % [m]
35
36 % Backplate thickness (rigid)
37 rigid_backplate_thk = max_liner_depth - (faceplate_thk + cavity1_depth + ...
38                               septum_thk      + cavity2_depth);
39
40 % Sanity check on total depth
41 sum_of_depths_m = faceplate_thk + cavity1_depth + septum_thk + ...
42                               cavity2_depth + rigid_backplate_thk;
43
44 disp(['Total liner depth is ', num2str(sum_of_depths_m*1e3, '%.3f'), ' mm']);
45 if sum_of_depths_m > max_liner_depth + 1e-9
46     warning('Liner thickness too large.');
47 end
48
49 %% ----- Helmholtz frequency band estimation -----
50 % MPP facesheet + cavity 1
51 f_H1 = (c0/(2*pi)) * sqrt(faceplate_phi/(cavity1_depth * L_eff_faceplate));
52
53 % Septum + cavity 2
54 f_H2 = (c0/(2*pi)) * sqrt(septum_phi/(cavity2_depth * L_eff_septum));
55
56 disp(['Frequency band 1 (f_H1) = ', num2str(f_H1, '.1f'), ' Hz']);
57 disp(['Frequency band 2 (f_H2) = ', num2str(f_H2, '.1f'), ' Hz']);
58
59 %% ----- Impedance Calculations -----
60 % Complex unit
61 j = 1i;
62
63 % --- Micro-perforated faceplate impedance (Bessel formulation) ---
64 x_faceplate      = (faceplate_d/2) * sqrt((-j*omega)/v0);
65 J0_faceplate    = besselj(0, x_faceplate);
66 J2_faceplate    = besselj(2, x_faceplate);
67 Z_MPP            = ((-j*k)./faceplate_phi) .* (J0_faceplate ./
68                   J2_faceplate);
69
70 % --- Cavity 1 input impedance (standalone) ---
71 Z_cavity1 = -j*z0 .* cot(k*cavity1_depth);
72
73 % --- Perforated septum impedance (Bessel formulation) ---
74 x_septum        = (septum_d/2) * sqrt((-j*omega)/v0);
75 J0_septum       = besselj(0, x_septum);
76 J2_septum       = besselj(2, x_septum);
77 Z_septum         = ((-j*k)./septum_phi) .* (J0_septum ./ J2_septum);
78
79 % --- Cavity 2 impedance (rigid termination) ---
80 Z_cavity2 = -j*z0 .* cot(k*cavity2_depth);
81
82 % --- DDOF combination via transfer (input) impedance ---
83 % Load at the end of cavity 1 (septum in series with cavity 2)
84 Z_load = Z_septum + Z_cavity2;
85
86 % Input impedance looking into cavity 1 terminated by Z_load:
87 % Z_in1 = Z0 * (Z_load*cos(kL1) - j*Z0*sin(kL1)) / (Z0*cos(kL1) -
88 %           j*Z_load*sin(kL1))
89 ck1 = cos(k*cavity1_depth);
90 sk1 = sin(k*cavity1_depth);
91 Z_in1 = Z0 .* (Z_load.*ck1 - j*Z0.*sk1) ./ (Z0.*ck1 - j*Z_load.*sk1);

```

```

90
91 % ----- Total Impedance -----
92 Z_total = Z_MPP + Z_inl;
93
94 %% ----- Acoustic Absorption -----
95 Gamma = (Z_total - Z0) ./ (Z_total + Z0); % Reflection coefficient
96 alpha = 1 - abs(Gamma).^2; % Absorption coefficient
97
98 avg_alpha = trapz(omega, alpha) / (omega(end) - omega(1));
99 disp(['Average absorption coefficient: ', num2str(avg_alpha, '%.4f')]);
100
101 %% ----- Plotting -----
102 figure('Color','w');
103 plot(f, alpha, 'LineWidth', 1.6); hold on;
104
105 % Mark estimated Helmholtz peaks (interpolate alpha at f_H1, f_H2 if in range)
106 if f_H1 >= f(1) && f_H1 <= f(end)
107 plot(f_H1, interp1(f, alpha, f_H1), 'o', 'MarkerFaceColor', 'r',
108      'DisplayName', 'f_{H1}');;
109 end
110 if f_H2 >= f(1) && f_H2 <= f(end)
111 plot(f_H2, interp1(f, alpha, f_H2), 'o', 'MarkerFaceColor', 'g',
112      'DisplayName', 'f_{H2}');;
113 xlabel('Frequency (Hz)', 'Interpreter','tex');
114 ylabel('Absorption Coefficient \alpha', 'Interpreter','tex');
115 title('Absorption Coefficient vs Frequency');
116 legend('Absorption curve', 'f_{H1}', 'f_{H2}', 'Location', 'best');
117 grid on; box on;
118
```

References

- [1] S. A. Rizzi. Urban air mobility noise: Current practice, gaps, and recommendations. Technical report, NASA Langley Research Center, 2020.
- [2] W. Raza and R. S. Stansbury. Noise prediction and mitigation for uas and evtol aircraft: A survey. *Drones*, 9(8):577, 2025.
- [3] K. Bakhet, B. Gaffney, B. Lee, E. McAleese, F. O'Connor, and M. Sadlier. Investigation of noise mitigation in urban air mobility: A review of acoustic liner concepts. Technical report, Trinity College Dublin, School of Engineering, 2025. 4E3 Research Methods, Group 17, Assignment 1.
- [4] A. Gautam, A. Celik, and M. Azarpeyvand. On the acoustic performance of double degree of freedom helmholtz resonator based acoustic liners. *Applied Acoustics*, 191:108661, 2022.
- [5] J. R. Kreitzman and M. G. Jones. Toward fully 3d-printed two degree of freedom acoustic liners. In *AIAA SCITECH 2024 Forum*, Orlando, FL, USA, 2024. American Institute of Aeronautics and Astronautics.
- [6] S. K. Tang, C. H. Ng, and E. Y. L. Lam. Experimental investigation of the sound absorption performance of compartmented helmholtz resonators. *Applied Acoustics*, 73(9):969–976, 2012.

- [7] M. B. Galles, D. M. Nark, M. G. Jones, and E. Greenwood. Optimization of variable depth acoustic liners with grazing flow. In *AIAA SCITECH 2024 Forum*, Orlando, FL, USA, 2024. American Institute of Aeronautics and Astronautics.
- [8] S. Palleja-Cabre, J. Ballgjati, C. Paruchuri, P. Joseph, and F. Avallone. Experimental investigation into the suppression of propeller noise using over-tip-rotor liners. In *Proc. AIAA/CEAS Aeroacoustics Conf.*, 2025. To appear.
- [9] Trinity College Dublin, School of Mechanical and Manufacturing Engineering. Research methods assignment 2 – research proposal. Module Blackboard site, Trinity College Dublin, oct 2025. Assignment brief for 4E3 Research Methods module. Accessed: 2 Nov. 2025.
- [10] C. Boutin. 1.02 – homogenization of high contrast media: From local physics to generalized continua. In V. Silberschmidt, editor, *Comprehensive Mechanics of Materials (First Edition)*, pages 4–44. Elsevier, Oxford, U.K., 2024.
- [11] P. Cobo, C. de la Colina, E. Roibás-Millán, M. Chimeno, and F. Simón. A wideband triple-layer microperforated panel sound absorber. *Composite Structures*, 226:111226, 2019.
- [12] A. N. Author. Folded cavity liners for turbofan engine intakes. In *AIAA/CEAS Aeroacoustics Conf.*, 2012. Preprint via ResearchGate.
- [13] D. L. Sutliff, D. M. Nark, and M. G. Jones. Multi-degree-of-freedom liner development: Concept to flight test. *International Journal of Aeroacoustics*, 20(5–7):792–825, 2021.
- [14] D. Y. Maa. Theory and design of microperforated panel sound-absorbing constructions. *Scientia Sinica*, 1975. English translation available via SciEngine.
- [15] A. McKay, I. Davis, J. Killeen, and G. J. Bennett. Semsa: A compact super absorber optimised for broadband, low-frequency noise attenuation. *Scientific Reports*, 10(1):17967, 2020.
- [16] A. N. Author. Evaluating an additive manufactured acoustic metamaterial using the advanced noise control fan. *AIAA Journal*, 2024. Early access.
- [17] M. Neubauer, J. Genßler, V. Radmann, F. Kohlenberg, M. Pohl, K. Böhme, K. Knobloch, E. Sarradj, K. Höschler, N. Modler, and L. Enghardt. Experimental and numerical investigation of novel acoustic liners and their design for aero-engine applications. *Aerospace*, 10(1):5, 2023.
- [18] Formlabs Inc. Technical data sheet – standard and engineering resins. Technical report, Formlabs, 2024.
- [19] B. M. Tymrak, M. Kreiger, and J. M. Pearce. Mechanical properties of components fabricated with open-source 3-d printers under realistic environmental conditions. *Materials & Design*, 58:242–246, 2014.
- [20] EOS GmbH. Material data sheet – aluminum alsi10mg for additive manufacturing. Technical report, EOS GmbH, 2023.
- [21] Stratasys Ltd. Performance characteristics of flexible and high-temperature photopolymers. Technical report, Stratasys, 2023.
- [22] S. Junk and F. Bär. Design guidelines for additive manufacturing using masked stereolithography (msla). *Procedia CIRP*, 119:1122–1127, 2023.
- [23] Madeleine P. What is the difference between sla and msla 3d printing?, August 2022. Accessed: 2 Nov. 2025.

- [24] J. W. Stansbury and M. J. Idacavage. 3d printing with polymers: Challenges among expanding options and opportunities. *Dental Materials*, 32(1):54–64, 2016.
- [25] A. Ciochon, J. Kennedy, and M. Culleton. Evaluation of surface roughness effects on additively manufactured acoustic materials. In *Proc. 30th ISMA International Conference on Noise and Vibration Engineering (ISMA2022)*, Leuven, Belgium, 2022.
- [26] S. Y. Song, X. H. Yang, F. X. Xin, S. W. Ren, and T. J. Lu. Modeling of roughness effects on acoustic properties of micro-slits. *Journal of Physics D: Applied Physics*, 50(23):235303, 2017.
- [27] A. Ciochon, J. Kennedy, R. Leiba, L. Flanagan, and M. Culleton. The impact of surface roughness on an additively manufactured acoustic material: An experimental and numerical investigation. *Journal of Sound and Vibration*, 546:117434, 2023.
- [28] A. Ciochon and J. Kennedy. Efficient modelling of surface roughness effects in additively manufactured materials. *Applied Acoustics*, 220:109953, 2024.

Minutes of Group Meetings

Meeting Date: 14/10/2019

Meeting Attendees: All group members.

6.2 Meeting 1 - Introductory Meeting

This meeting was organised to begin brainstorming the assignment, assign initial roles, and gather feedback on each member about how we thought assignment 1 went. The aims of the meeting were:

- Analyse strengths, weaknesses, what went well, and what didn't from assignment 1.
- Brainstorm ideas for assignment 2.
- Develop a project timeline.
- Assign roles for each member.

Discussion Points:

| Ref | Discussion |
|-----------------------|--|
| Assignment 1 Analysis | Research, referencing, and final document formatting were our strengths. Communication between members sharing parts was poorly co-ordinated. |
| Project Timeline | Weekly meetings every Tuesday, consistent communication for members working collaboratively on each part. Project to be finished, ready to submit. |
| Team Roles | Michael - CAD (20%) Billy - Manufacturing (15%) Finn and Karim - Physics and basis of design (25%) Brian - High level description based on literature review (15%) Emily - Risk assessment (15%) |

Actions:

| No. | Description | Responsible | Due | Note |
|-----|--|-------------------|------------|--|
| 1 | Timeline development to be agreed upon | All Group Members | 14/10/2025 | Project to be finished by 28/10/2025 |
| 2 | Initial research to be finished | All Group Members | 20/10/2025 | Research uploaded to collaborative Word document; at least three references from each member |
| 3 | Model design to be decided upon | All Group Members | 20/10/2025 | Model to be built, drawings compiled, and STL files created |

Table 4: Meeting actions and deadlines.

Meeting Date: 21/10/2019

Meeting Attendees: All group members.

6.3 Meeting 2 - Design Clarification and Progress Updates

This meeting was organised to clarify our final design, show sketches, and explain the working of our proposed design, based off the results from our Assignment 1, and our initial desk research:

- Clarify final design.
- Begin writing individual sections.
- Share references already collated.

Discussion Points:

| Ref | Discussion |
|----------------------|---|
| Design Clarification | Ensure each group member has a clear knowledge on our design, and understands it well. |
| Reference Collection | Share references already in use for assignment 2, update members on references that will be used in both assignments. |
| Report Writing | Update the group on progress made on each member's section in the report, and explain what had been written thus far. |

Actions:

| No. | Description | Responsible | Due | Note |
|-----|----------------------|-------------------|------------|--------------------------------|
| 1 | Report Finished | All Group Members | 28/10/2025 | Report entirely finished |
| 2 | References Finalised | All Group Members | 24/10/2025 | Ensures Zotero file management |

Table 5: Meeting actions and deadlines.

6.4 Meeting 3 - Final Review and Submission Planning

Meeting Date: Friday, 31/10/2025

Attendees: All group members.

This meeting was organised to confirm what needed to be done in order to submit the final report. The focus was on formatting, referencing consistency, proofreading, and final checks before submission. Having received feedback from assignment 1, we wanted to ensure that we implemented the necessary changes to elevate our grade.

- Final formatting of the report.

- Reference list cleanup (DOIs, consistent style).
- Final proofreading and technical accuracy check.
- Confirm submission responsibilities and timeline.

Discussion Points:

| Ref | Discussion |
|--------------|---|
| Formatting | Agreed on consistent figure styles, table layouts, captions, and section numbering. All blurred/low-resolution figures to be replaced or redrawn at sufficient quality. |
| Referencing | Confirmed that all references must follow IEEE style with initials only, DOIs included where possible, and no missing publication details. Zotero/BibTeX entries to be normalised and recompiled. |
| Proofreading | Each section to be read by at least one person who did <i>not</i> write it, to remove typos, fix repetition, and check that claims are supported by citations with quantitative backing where possible. |
| Submission | Final PDF generation, final contents page check, and upload procedure were agreed. Responsibility for upload assigned. |

Actions:

| No. | Description | Responsible | Due | Note |
|-----|--|-------------------|-----------|--|
| 1 | Full formatting pass (figures, tables, captions) | Michael & Finn | 2/11/2025 | Replace low-res figures, table of contents, and fix layout issues. |
| 2 | Finalise bibliography (IEEE style, DOIs, consistent author initials) | Finn | 2/11/2025 | Clean .bib file and recompile. |
| 3 | Proofread full draft | All Group Members | 2/11/2025 | Spelling/grammar and check for unsupported claims. |
| 4 | Final PDF export and submission | Finn | 2/11/2025 | Confirm correct version uploaded before deadline. |

Table 6: Actions agreed during Meeting 3.

7 CRediT Author Statement

- **K. Bakhet** – Sections 3.1. Physical Properties of Materials. Ref 16, 17, 18, 19, 20.
- **B. Gaffney** – Sections 1, 1.1, 1.2, 1.3. Ref 1, 2, 3, 4, 5, 6, 7, 8. Introduction, Meeting Minutes 1 and 2
- **B. Lee** – Sections 3.1, 3.2, 3.3. Manufacturing Strategy. Ref 17, 22, 23, 16.
- **E. McAleese** – Sections 5, 5.1, 5.2 5.3. Risk Assessment. Ref 22, 24, 25, 26, 27, 28.
- **F. O'Connor** – Sections 2.1, 2.2, 2.3, 2.4, 2.5, 2.6, 2.7. Physics, Sketches, MATLAB model, Meeting Minutes 3, Formatting. Ref 9, 10, 11, 12, 13, 14, 15, 16.
- **M. Sadlier** – Sections 4.1, 4.2, 4.3, 4.4. CAD.

8 Generative AI Declaration

Group 17 declares that no form of generative artificial intelligence (GenAI) was used to create the content, figures, or analysis within this report. The work submitted is 100% human.

9 Group Grade Scaling Factor

K. Bakhet : 100%

B. Gaffney: 100%

B. Lee: 100%

E. McAleese: 100%

F. O'Connor: 100%

M. Sadlier: 100%